Design & Optimization of the Spherical Primary Optical Telescope (SPOT) Primary Mirror Segment

Jason G. Budinoff[1], Gregory J. Michels[2]
[1]NASA GSFC Code 544 8800 Greenbelt Rd, Greenbelt MD 20771
[2]Sigmadyne, Inc., 803 West Avenue, Rochester, NY 14611

1. ABSTRACT

The 3m Spherical Primary Optical Telescope (SPOT) will utilize a single ring of 0.86m point-to-point hexagonal mirror segments. The f2.85 spherical mirror blanks will be fabricated by the same replication process used for mass-produced commercial telescope mirrors.

Diffraction-limited phasing will require segment-to-segment radius of curvature (ROC) variation of ~1 micron. Low-cost, replicated segment ROC variations are estimated to be almost 1 mm, necessitating a method for segment ROC adjustment & matching. A mechanical architecture has been designed that allows segment ROC to be adjusted up to 400 microns while introducing a minimum figure error, allowing segment-to-segment ROC matching. A key feature of the architecture is the unique back profile of the mirror segments.

The back profile of the mirror was developed with shape optimization in MSC.Nastran™ using optical performance response equations written with SigFit. A candidate back profile was generated which minimized ROC-adjustment-induced surface error while meeting the constraints imposed by the fabrication method.

Keywords: optimization, radius of curvature, Pyrex spherical mirror, Sigfit

2. INTRODUCTION

2.1 System Description & Requirements

The Spherical Primary Optical Telescope (SPOT) is a GSFC internal research & development program initiated in 2003. The goal of the SPOT effort is to develop a robust architecture which will reduce the cost of large-aperture, segmented primary mirror space telescopes. The SPOT telescope architecture is based upon 2 key technology developments: a high-rate, center of curvature, phase-diversity phasing algorithm, and a low-cost mirror segment. This paper presents the optimization of the low-cost mirror segment's unique back profile.

The SPOT demonstration telescope is a ∅3m segmented spherical primary. The primary consists of 6 identical hexagonal segments measuring 876 mm point-to-point, in a 1-ring configuration, without a central segment. However, only 2 segments are being fabricated for this effort. Two segments are the minimum amount required to successfully demonstrate the phasing architecture. Each segment has rigid-body position control in tip, tilt, and piston. Each segment also has mechanical radius-of-curvature control. Some of the relevant requirements[1] for the SPOT mirror segments are given in the following table:

Table 1: Pyrex™ Mirror Segment Requirements

Requirement	Value	Units	Note
Size	∅876 (34.5)	mm (inch)	Point-to-point hex
Radius of curvature (ROC)	5000 ± 0.20	mm	Measured before plating
Figure	1/30	waves@633nm	ambient
Surface Roughness	40	Angstrom	
ROC adjustment range	±400	microns	
ROC adjustment resolution	1	micron	
Max Surface error for 400 micron ROC adjustment	15	nm RMS	
Thermal Operational Environment	20-26	Degrees C	ambient

There are two key technologies that SPOT is pursuing to develop a low-cost mirror segment: a replicated (cast) Pyrex blank process and mechanical ROC control. The ROC control is required as part-to-part ROC variations from this process are expected to be hundreds of microns.

2.2 Mirror Fabrication

Commercial reflecting telescopes of 6-14 inch aperture typically use Pyrex replicated mirrors. The Pyrex replication process involves pressing a boule of viscous molten Pyrex at ~900°C into a cast iron mold of the mirror back. After removal from the mold, a several-week controlled cooling process results in a fine-annealed, near-net-shape blank, ready to be ground & figured. This process has been in use for over 70 years and is well understood, and scalable to meter-class segments using existing production equipment.

2.3 Design Limitations Imposed by the Replication Process

A mirror designed for fabrication by the Pyrex replication process has to follow some basic guidelines applicable to any cast solid. The thickness of the mirror blank should remain between 10 and 100 mm to reduce differential cooling stress in the blank, and guarantee that the Pyrex presses completely into the mold cavity. Molten Pyrex has the consistency of soft butter. It is not a viscous liquid and does not flow which is why it must be pressed into the mold cavity. This non-flowing property means that any stiffening features, such as radial ribs, must not be too thin or too high else the Pyrex may not press into them completely and differential cooling in the thinnest sections may overstress the part. The edge of the mirror must have a draft angle (typically 5 degrees or more) to facilitate mold release. Lightweighting features such as pocket patterns cannot be very deep and must have a significant draft angle (again 5+ degrees) which reduces their effectiveness.

3. MECHANICAL RADIUS OF CURVATURE ADJUSTMENT

3.1 The Importance of ROC Matching

For a segmented mirror to produce a diffraction-limited image comparable to an equivalent monolithic, each segment's ROC must match the parent surface ROC to better than 1 micron. For replicated, meter-class borosilicate mirrors not cut from a common parent, radius of curvature variations are expected to be hundreds of microns. To fabricate individual (not cut from a common parent) segments which are ROC-matched to better than 1 micron is cost-prohibitive.

3.2 ROC Adjustment System

The ROC adjustment architecture consists of a mechanical spider which grasps the back of the mirror at 12 points around the edge perimeter. The radial struts which comprise the spider's "legs" are connected to a central post, which is rigidly attached to the center back of the mirror. The central post contains a single linear actuator which changes its length to vary the strut tension. This allows the edges to be reacted against the center of the mirror. The system as initially designed is illustrated in figure 1.

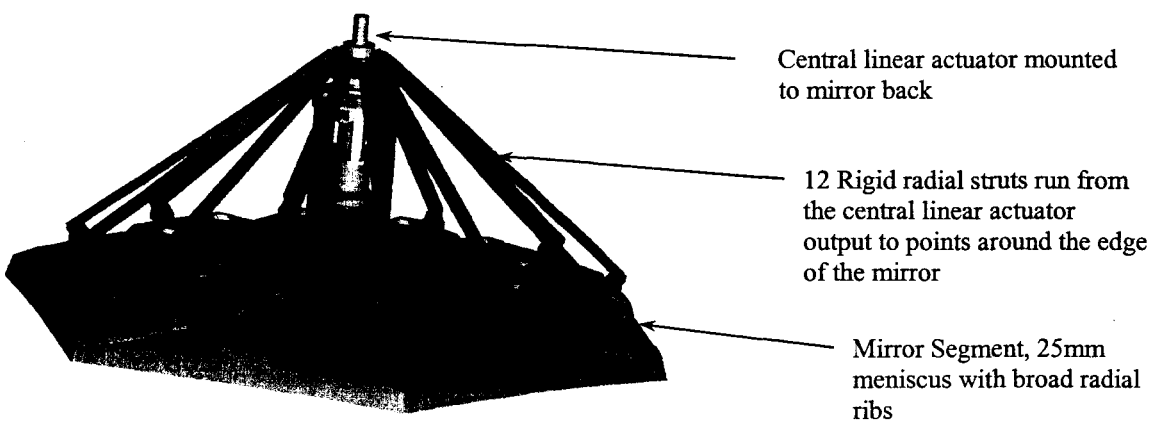

Figure 1: Radius of curvature adjustment system conceptual layout

4. FEA ANALYSIS AND OPTIMIZATION

4.1 Analysis of Initial Design

A model of the initial design was constructed in MSC.Nastran™,[2] using 10-noded CTETRA elements to represent the mirror and beam elements to represent the actuator struts. The actuator was modeled of rigid elements with the capability to enforce motion between the upper and lower actuator parts. Figure 2 shows a plot of this model.

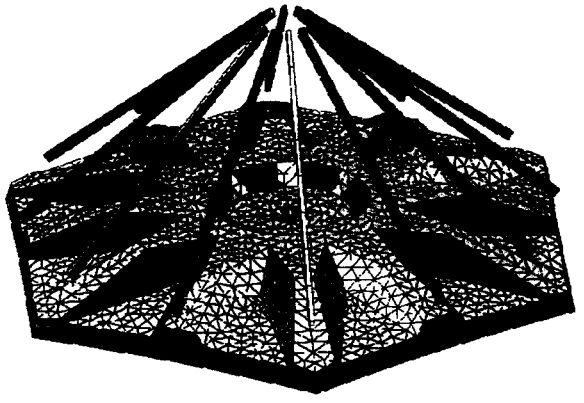

Figure 2: Plot of finite element model for initial design.

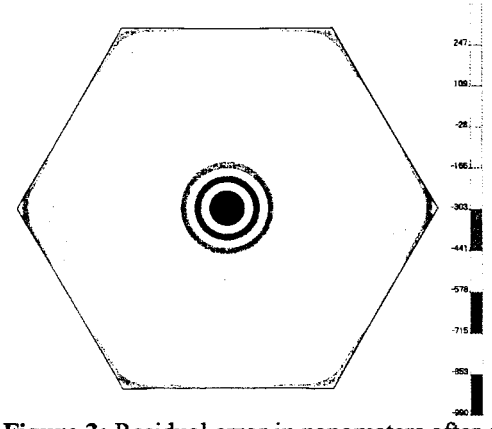

Figure 3: Residual error in nanometers after correction for the initial design.

Using the finite element predictions of the actuator influence function Sigmadyne/SigFit was used to simulate adaptive control of a 2 mm radius-of-curvature change. The initial design is predicted to correct the 2 mm radius-of-curvature change with a residual surface error of 225 nm and a residual P-V error of 1237 nm. A plot of the residual surface error after best correction is shown in Figure 3. Notice that the use of ribs in the mirror design is relatively effective in controlling azimuthally varying deformations. However, the shape of the structural design along the radial direction is preventing the optical surface from deforming to a new spherical shape. When scaled to a 400 micron ROC correction, this design produces 45 nm of RMS surface error, exceeding the allocation of 15 nm.

4.2 Design Variables & Constraints

For the design optimization, the back surface of the mirror was allowed to contour. The shape of this contoured surface was first defined by an axisymmetric polynomial surface of revolution. The polynomial definition defines the axial location of the surface relative to the plane at the mirror vertex. The equation for this surface expressed in millimeters is given in equation (1),

$$f(r) = a_0 + a_1\frac{r}{437.728} + a_2\left[\frac{r}{437.728}\right]^2 + a_3\left[\frac{r}{437.728}\right]^3 + a_4\left[\frac{r}{437.728}\right]^4, \tag{1}$$

where, the coefficients a_0, a_1, a_2, a_3 and a_4 are design variables and r is expressed in millimeters. Notice that the coefficient a_0 is the center thickness (r = 0) while the remaining terms define how the shape of the back surface varies with radius.

A second shaping scheme was also developed in which the back surface was defined by a two-dimensional 4th order polynomial/harmonic function as defined in Equation (2).

$$\begin{aligned} f(r,\theta) = {} & a_0 + a_1\frac{r}{437.728} + a_2\left[\frac{r}{437.728}\right]^2 + a_3\left[\frac{r}{437.728}\right]^3 + a_4\left[\frac{r}{437.728}\right]^4 + \\ & b_1\left[\frac{r}{437.728}\right]\cos(6\theta) + b_2\left[\frac{r}{437.728}\right]^2\cos(6\theta) + b_3\left[\frac{r}{437.728}\right]^3\cos(6\theta) + b_4\left[\frac{r}{437.728}\right]^4\cos(6\theta) + \\ & c_1\left[\frac{r}{437.728}\right]\cos(12\theta) + c_2\left[\frac{r}{437.728}\right]^2\cos(12\theta) + c_3\left[\frac{r}{437.728}\right]^3\cos(12\theta) + c_4\left[\frac{r}{437.728}\right]^4\cos(12\theta) \end{aligned} \tag{2}$$

Notice that this shaping scheme contains the same radial variation capability as in Equation (1) but with additional variations which allow for variation in the azimuthal direction. The terms with *cos(6θ)* cause six-fold azimuthal shaping while the terms with *cos(12θ)* cause twelve-fold azimuthal shaping. The combination of the two allows adjacent ribs to be different heights. This allows the optimization to find 2 unique rib heights for struts attaching at the corners and struts attaching at the sides of the hexagon. Such a shape is shown in Figure 4.

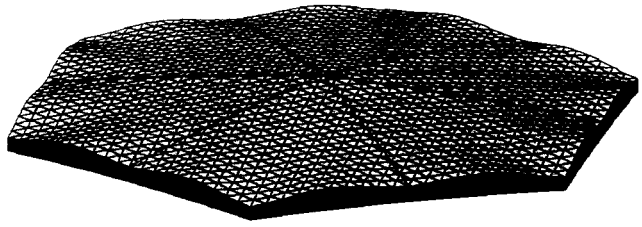

Figure 4: Plot of finite element model showing possible shape generated by use of Equation (2).

However, the shape above does not have a central flat region with which the mirror may be mounted for figuring. Therefore, a third optimization was performed to include such a feature. The shape of this contoured surface was defined by a central flat region 254.0 mm in diameter and a 4th order polynomial/harmonic function in 2 dimensions outside of this diameter as shown in Equation (3).

$$f(r,\theta) = a_0 \quad r \le 127\ mm$$

$$f(r,\theta) = a_0 + a_1\frac{(r-127)}{310.728} + a_2\left[\frac{(r-127)}{310.728}\right]^2 + a_3\left[\frac{(r-127)}{310.728}\right]^3 + a_4\left[\frac{(r-127)}{310.728}\right]^4 + \tag{3}$$

$$b_1\left[\frac{(r-127)}{310.728}\right]\cos(6\theta) + b_2\left[\frac{(r-127)}{310.728}\right]^2\cos(6\theta) + b_3\left[\frac{(r-127)}{310.728}\right]^3\cos(6\theta) + b_4\left[\frac{(r-127)}{310.728}\right]^4\cos(6\theta) +$$

$$c_1\left[\frac{(r-127)}{310.728}\right]\cos(12\theta) + c_2\left[\frac{(r-127)}{310.728}\right]^2\cos(12\theta) + c_3\left[\frac{(r-127)}{310.728}\right]^3\cos(12\theta) + c_4\left[\frac{(r-127)}{310.728}\right]^4\cos(12\theta)$$

Thickness constraints were applied to the shape of the mirror so that the axial thickness nowhere exceeds 101.6 mm (4 inches) and is nowhere less than 10.0 mm due to the limits imposed by the fabrication process.

In addition to the shaping the back surface, the orientations of the struts were also used as design variables. While the location of the attachment of each strut to the actuator unit was kept the same, the axial locations of the strut ends that attach to the mirror edges were allowed to vary. While 1 design variable controlled the orientation of the struts attaching to the corners of the mirror, a second independent variable was used to control the orientation of the struts attaching to the straight edges of the mirror. Figure 5 illustrates such a change in strut orientation.

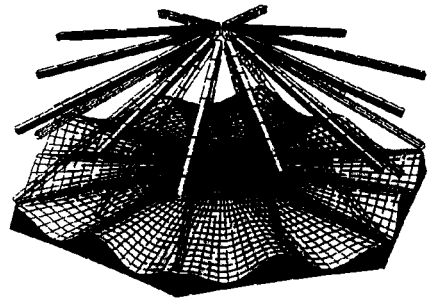

Figure 5: Plot of finite element model showing change in strut orientation.

4.3 Optimization Results

Optimum designs were found for each of the 3 shaping equations presented above. For each shaping scheme optimizations were performed with and without variable strut orientation. The residual corrected surface RMS and P-V errors for the initial design and each optimized design are shown in Table 2. Final analyses using the optimum designs from the shaping scheme defined by Equation (3) were performed including a 10 degree draft angle on the edge of the mirror. The draft is required but could not be included easily in the shape optimizations.

Table 2: Corrected Surface RMS Error Predictions for 2 mm ROC Change

	Strut End Offsets Fixed		Strut End Offsets Allowed to Vary	
Design	**Corrected Surface RMS Error**	**Corrected Surface P-V Error**	**Corrected Surface RMS Error**	**Corrected Surface P-V Error**
Rev. G (No Optimization)	225 nm	1236.9 nm		
Optimized Axisym Design With No Central Flat (Equation 1)	36.0 nm	331.8 nm	22.1 nm	196.8 nm
Optimized Non-Axisym Design With No Central Flat (Equation 2)	30.9 nm	285.3 nm	20.6 nm	188.0 nm
Optimized Non-Axisym Design With Central Flat (Equation 3)	40.5 nm	233.3 nm	30.6 nm	198.3 nm
Beveled Optimized Design With Central Flat	44.7 nm	257.9 nm	32.5 nm	204.7 nm

Figures 6a and 6b show plots of the surface errors for the optimum design using Equation (2) and Equation (3), respectively. Recall that while the shaping defined by Equation (3) includes a central flat area required for processing of the mirror, the shaping defined by Equation (2) contains no central flat area.

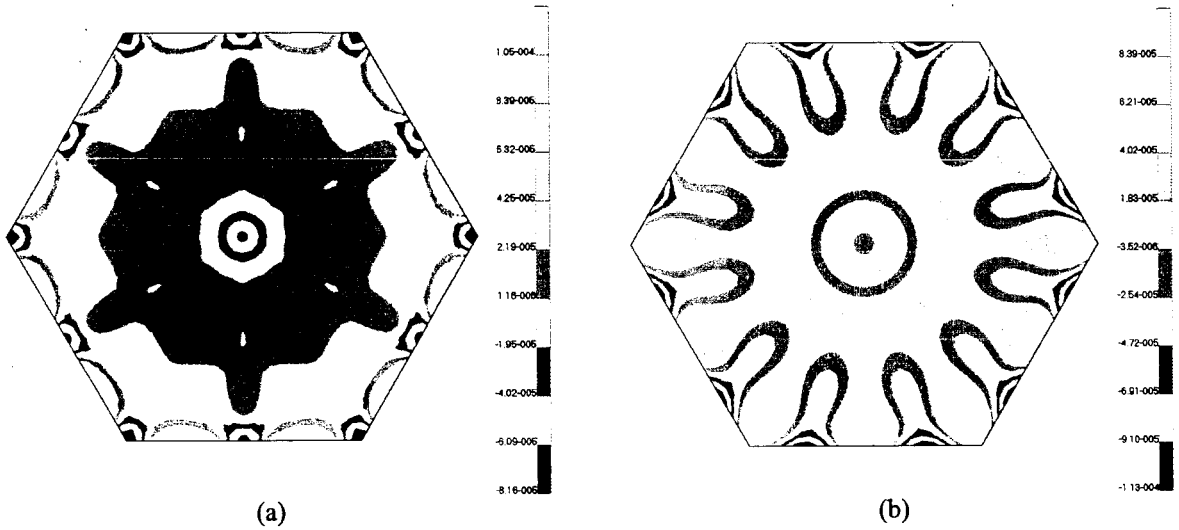

(a) (b)

Figure 6: Plots of surface error in nanometers after best correction for optimum designs (a) without central flat and (b) with central flat.

Notice that omission of the central flat in the mirror design allows the optimizer to find an optimum design whose residual error is dictated by the local effects of the strut attachments. However, inclusion of the central flat presents a measurably more difficult optimization problem resulting in 49% greater corrected surface error than if the central flat is omitted.

Figures 7a and 7b show plots of the finite element models of the optimized designs using the shaping schemes defined by Equations (2) and (3), respectively.

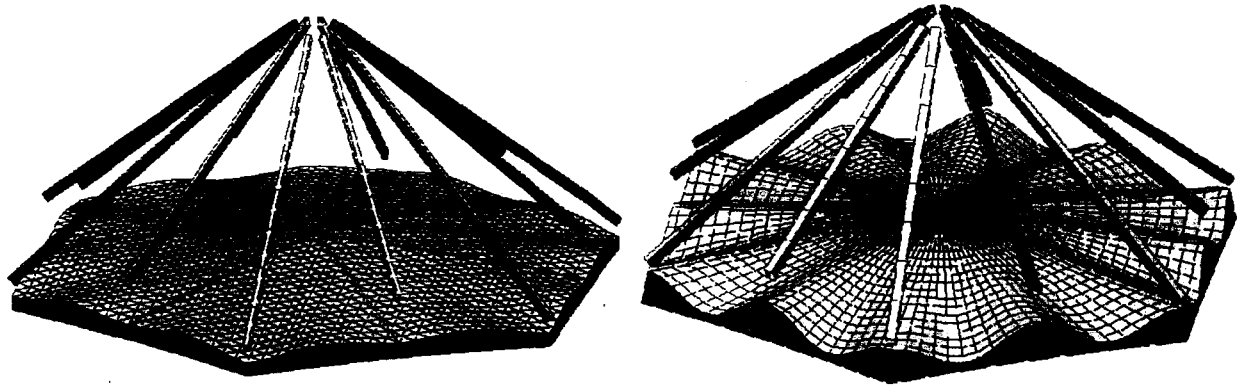

(a) (b)

Figure 7: Plots of finite element models of optimum designs from shaping schemes defined by (a) Equation (2) and (b) Equation (3).

5. CONCLUSIONS

An optimized mirror back profile which allows a 2 mm mechanical radius of curvature adjustment has been analyzed. This profile minimizes RMS surface error induced by the mechanical ROC adjustment. When scaled to a 400 micron ROC adjustment, the RMS surface error is 6.5 nm, well below the 15 nm allocation. These numbers could be improved by introducing additional shaping terms in the regions of the strut attach points.

The family of surfaces produced by the shaping optimizations represents a first step in the development of stressed-surface, adjustable radius-of-curvature mirrors. The mirror design performance will be verified later this year as the mirror segment and ROC adjustment architecture is fabricated and tested.

6. REFERENCES

1. J. Budinoff, SPOT Mirror Segment Assembly Requirements - Revision C, March 2004
2. NASTRAN™ is a registered trademark of the National Aeronautics and Space Administration. MSC.Nastran™ is a registered trademark of the MSC.Software corporation.